Bond-dissociation energies to probe pyridines electronic effects on organogold(III) complexes: from methodological developments to application in π-backdonation investigation and catalysis

Lyna Bourehil, Clément Soep, Sopheak Seng, Sarah Dutrannoy, Stacy Igoudjil, Jérémy Forté, Geoffrey Gontard, Denis Lesage, Benoît Bertrand, Héloïse Dossmann

Bond dissociation energies to probe pyridines electronic effects on organogold(III) complexes: from methodological developments to application in π-backdonation investigation and catalysis

Lyna Bourehil,[a,b] Clément Soep,[a] Sopheak Seng,[a,c] Sarah Dutrannoy,[a] Stacy Igoudjil,[a] Jérémy Forté,[a] Geoffrey Gontard,[a] Denis Lesage,[a]* Benoît Bertrand[a]* and Héloïse Dossmann[a]*

[a] Sorbonne Université, CNRS, Institut Parisien de Chimie Moléculaire, IPCM, F-75005 Paris, France

[b] Synchrotron SOLEIL, L'Orme des Merisiers, St Aubin, BP 48, F-91192 Gif-sur-Yvette, France

[c] Institute of Physical Chemistry, Karlsruhe Institute of Technology (KIT), Fritz-Haber-Weg 2, D-76131 Karlsruhe, Germany

ABSTRACT: In this work, we report on the synthesis of several organogold(III) complexes based on 4,4'-diterbutylbiphenyl (C^C) and 2,6-bis(4-terbutylphenyl)pyridine (C^N^C) ligands and bond with variously substituted pyridine ligands (pyrR). Altogether 33 complexes have been prepared and studied with mass spectrometry using higher-energy collision dissociation (HCD) in an Orbitrap mass spectrometer. A complete methodology including the kinetic modeling of the dissociation process based on the Rice-Ramsperger-Kassel-Marcus (RRKM) statistical method is proposed to obtain critical energies E_0 of the pyrR loss for all complexes. The capacity of these E_0 values to describe the pyridine ligand effect is further explored, at the same time as more classical descriptors such as ^{1}H pyridinic NMR shift variation upon coordination and X-ray diffraction measured Au-N^{pyrR} bond length. An extensive theoretical work, including density-functional theory (DFT) and domain-based local pair natural orbital coupled-cluster theory (DLPNO-CCSD(T)) methods, also is carried out to provide bond-dissociation energies which are compared to experimental results. Results show that dissociation energy outperforms others descriptors, in particular to describe ligands effects over a large electronic effects range as seen by confronting the results to the pyrR pK_as values. Further insights into the Au-N^{pyrR} bond are obtained through an Energy-Decomposition Analysis (EDA) study which confirms the isolobal character of Au^+ with H^+. Finally, the correlation between the lability of the pyridine ligands towards the catalytic efficiency of the complexes could be demonstrated in an intramolecular hydroarylation reaction of alkyne. The results were rationalized considering both pre-catalyst activation and catalyst reactivity. This study establishes the possibility of correlating dissociation energy, which is a gas-phase descriptor, with condensed-phase parameters such as catalysis efficiency. It holds therefore great potential for inorganic and organometallic chemistry by opening a convenient and easy way to evaluate the electronic influence of a ligand towards a metallic center.

Through their steric and electronic effects, ligands play a crucial role in inorganic chemistry, with direct implications in organometallic catalysis, biomedicine or material science.[1, 2] They influence the net electron density on the metallic center and constrain the access to the first coordination sphere. They are therefore able to drive its behavior and reactivity, leading for instance to high selectivity in chemical transformations. To access fine tuning of catalytic reaction pathways or material design a detailed knowledge of metal ligand interactions may thus be required in order to evaluate the steric and electronic influence of the latter. The classical model depicting electronic interactions between a metal and a ligand is the Dewar-Chatt-Duncanson model[3] which involves σ / π -donor and -acceptor capabilities of the ligand resulting in a global metal-ligand interaction. Over the years, many experimental methods and descriptors have been developed to evaluate the electronic effects resulting from the coordination of a ligand to a metal. One of the most well-known approach is the Tolman electronic parameter (TEP) applied to organometallic complexes possessing CO probe ligands and based on the determination of their infrared A_1-symmetrical CO-stretching frequency.[4] TEP has enabled the classification of phosphine ligands according to their donating capacity and was also extended to the classification of N-heterocyclic carbenes (NHCs) using [Ir/$Rh(CO)_2Cl(L)$] complexes.[5] Another descriptor, the Huynh Electronic Parameter (HEP), implies ^{13}C NMR spectroscopy and relies on the determination of the chemical shift of the carbenic carbon of a NHC ligand in *trans*-[(NHC)$PdCl_2(L)$] and $[(NHC)AuL]^+$ complexes.[6] The donation strengths of various types of ligands were determined in this way, including NHCs, phosphines and N-donor ligands. Furthermore, Rocchigiani and Bochmann used the ^{1}H NMR chemical shift of hydride ligands in organogold(III) complexes to study the *trans*- and *cis*-influence of various ligands, including (C^N), (C^C), (C^N^C) and (C^C^N) chelates.[7] Eventually, gas-phase studies have also been involved in this field with, for instance, the use of ionization energies[8-10] or bond-dissociation energies (BDEs)[11, 12] as descriptors of the ligand electronic effects. Recently, our group was thus implicated in a project aiming at the evaluation of the ligand strengths in a series of $[L\text{-}Au\text{-}CO]^+$ complexes (L being a phosphine, phosphite or NHC ligand) using Au-CO BDEs determined by two mass spectrometry (MS) - based methodologies, Blackbody Infrared Radiative Dissociation (BIRD)[13] and collision-induced dissociation (CID) in the multi-collisional regime.[14] With a similar approach to Tolman's, we determined that the variation of the Au-CO bonding energy could be linked to the ligands' electronic properties and that BDE could accordingly serve as a valuable descriptor for these effects.

Although usually performing well, all the above-cited experimental approaches rely on the use of a probe ligand such as C≡O for Tolman/BDE and a N-heterocyclic carbene (NHC) for Huynh parameter. The need for such specific ligands dramatically limits the range and diversity of the systems to be studied but may also lead to a lack of sensitivity, making such approach difficult to generalize. We thus endeavored to develop a new methodology free of such constraint. In the present project, we propose the investigation of the electronic influence of variously substituted pyridines bound to several Au(III) scaffolds using bond-dissociation energy measurements of the Au-N^{pyrR} bond. The systems were designed without probe ligands and the unique imposed constraint was the lability of the pyridines in order to access the bonding energy. The designed gold (III) complexes are 33 and of the $[(C\hat{}C)Au(NHC/PPh_3)L]^+$ and $[(C\hat{}N\hat{}C)AuL]^+$ type with L being the pyridine ligand of interest (Scheme 1). These (C^C) and (C^N^C) chelating ligands are known for their high stability[15, 16] and a large panel of applications in fundamental organometallic chemistry,[17, 18] photoluminescence[19-21] and biology.[15, 22] Three scaffolds were chosen in order to access a large range of electronic effect. Aryl ligands (complexes **1** and **2**) are indeed known to have a higher *trans* influence compared to N-donor ligands (complexes **3**).[23]

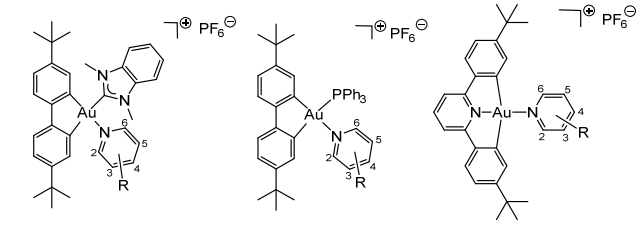

[(C^C)Au(NHC)(pyrR)]$^+PF_6^-$ **1PF6**

R = **1a** 4-NMe_2 (93%) **1b** 4-OMe (87%) **1c** 4-Me (98%) **1d** 4-Ph (93%) **1e** H (90%) **1f** 4-Ac (98%) **1g** 4-CO_2Et (84%) **1h** 4-CF_3 (94%) **1i** 4-CN (90%) **1j** 3-OMe (86%) **1k** 3-Me (85%) **1l** 3-CF_3 (81%) **1m** 2-OMe (92%) **1n** 2-Me (94%)

[(C^C)Au(PPh_3)(pyrR)]$^+PF_6^-$ **2PF6**

2a 4-NMe_2 (85%) **2e** H (86%) **2f** 4-Ac (78%) **2h** 4-CF_3 (58%) **2i** 4-CN (84%)

[(C^N^C)Au(pyrR)]$^+PF_6^-$ **3PF6**

3a 4-NMe_2 (70%) **3b** 4-OMe (88%) **3c** 4-Me (72%) **3d** 4-Ph (91%) **3e** H (75%) **3f** 4-Ac (72%) **3g** 4-CO_2Et (84%) **3h** 4-CF_3 (80%) **3i** 4-CN (61%) **3j** 3-OMe (85%) **3k** 3-Me (78%) **3l** 3-CF_3 (73%) **3m** 2-OMe (79%) **3n** 2-Me (72%)

Scheme 1. Structures of the 33 studied organogold(III) complexes. The reaction yield is indicated in brackets for each R substituent. The numbers on the pyridine indicate the R position.

The effect of pyridine substitution on the metal enrichment was evaluated by determining the dissociation energy $[[Au]\text{-}N^{pyrR}]]^+ \rightarrow [Au]^+ + N^{pyrR}$ ([Au] being one of the three scaffolds) using higher-energy collision dissociation (HCD) available on an Orbitrap mass spectrometer. A statistical Rice-Ramsperger-Kassel-Marcus (RRKM)[24-27] modeling was performed to determine the critical energy (E_0) of the fragmentation and compared with several theoretical approaches, including density-functional theory (DFT) and *ab initio* methods as well as energy decomposition analysis (EDA). This newly-developed bond-energy descriptor was compared to classical ones, i.e. X-ray diffraction bond lengths and ^{1}H(pyrR) NMR shifts variation upon coordination and all rationalized by means of the pK_a values of the free pyridines. Interestingly, the bond-dissociation energies appear much more efficient and reliable to describe the electronic influence of the pyridines over the very large electronic effects probed range. In the light of these results, the isolobality of the Au(III) fragments with H^+ is discussed as well as the π-acceptor contribution on the Au-pyrR interaction. Finally, a first step to link this gas-phase descriptor to the condensed-phase reactivity of the complexes is done by probing their catalytic activity in an intramolecular hydroarylation reaction of alkyne and rationalizing it in the view of the Au-N^{pyrR} bond strength.

RESULTS AND DISCUSSION

Synthesis of the complexes.$[(C\hat{}C)Au(NHC)(pyrR)]PF_6$ complexes **1a-nPF6** were synthetized in two steps. First, the 1,3-dimethylbenzimidazol-3-ylidene (NHC) ligand was introduced onto the [(C^C)AuCl] moiety by using the silver-based transmetallation method with the $[(C\hat{}C)AuCl]_2$ dimer to form the [(C^C)Au(NHC)Cl] complex **1**.[28] In a second step, the chlorido ligand was abstracted using silver hexafluorophosphate and replaced by variously substituted pyridines in para, meta and ortho position with excellent yields (Scheme 1). $[(C\hat{}C)Au(PPh_3)(pyrR)]PF_6$ complexes **2a, e, f, h** and **iPF6** were synthesized *via* a one-pot two-steps procedure starting by the introduction of the substituted pyridine onto the [(C^C)AuCl] scaffold followed by the abstraction of the chlorido ligand using silver hexafluorophosphate and the introduction of the triphenylphosphine ligand with satisfying to very good yields (Scheme 1). The $[(C\hat{}N\hat{}C)Au(pyrR)]PF_6$ **3a-nPF6** were synthesized from the [(C^N^C)AuCl] precursor by a modified reported procedure involving the abstraction of the chlorido ligand using silver hexafluorophosphate and introduction of the substituted pyridines with good to excellent yield.

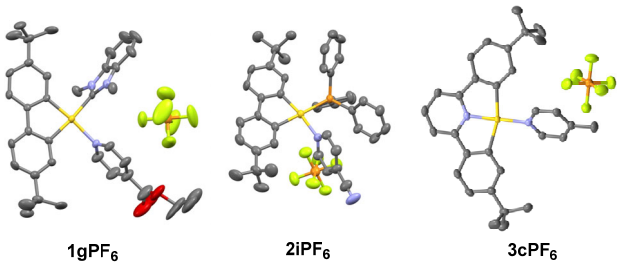

1gPF6 **2iPF6** **3cPF6**

Figure 1. Crystal structures obtained for each of the three scaffolds: **1gPF6**, **2iPF6** and **3cPF6**. Ellipsoids are set at 50% probability and hydrogen atoms omitted for clarity (and dichloromethane for **3cPF6**). Only one complex of the asymmetric unit is shown for **1gPF6** and **2iPF6**. All XRD structural parameters are detailed in the SI (Figs. S1-S17).

X-ray diffraction analysis. As a first probe of the donating capability of the pyridines towards the metal, a close inspection of the structural parameters may serve as a good indicator. Crystal structures of a large number of the studied complexes were obtained and are shown in Figs 1 and S1-17 and the Au-N^{pyrR} bond lengths are given in Table S1 and Fig. 2. The structures of **1**, **2** and **3** series present the typical square-planar 4-coordinated geometry of Au(III) complexes with small distortions according to the chelating ligands used in agreement with reported data for (C^C)- and (C^N^C)-based Au(III) complexes.[28-30] Replacement of the chlorido ligand by the substituted pyridines in the $[(C\hat{}C)Au(NHC)]^+$ series does not modify the bond length and angles for the (C^C) and NHC ligands. In all $[(C\hat{}C)Au(PPh_3)(pyrR)]PF_6$ **2PF6** structures, the pyridine ligand appears almost parallel to a phenyl ring of the PPh_3 placing the pyridine protons in the anisotropy cone of the phenyl ring explaining the shielding of this proton upon coordination observed by ^{1}H NMR spectroscopy (see below). To evaluate the metal-ligand bond strength, the Au-N^{pyrR} bond lengths were considered (Table S1, Fig. 2). The first observation concerns the (C^N^C)-based complexes **3PF6** which present a significantly shorter Au-N^{pyrR} bond length compared to (C^C)-based

1PF$_6$ and **2PF$_6$** complexes (around 2.05 Å *vs.* 2.13 Å, respectively).

This observation is in agreement with the known *trans* influence applied by N-donor ligands compared to aryl ones.[23] *Trans* influence of ligands indeed defines the electron-donating capability of a ligand towards the metal which results in the weakening of the bond between the metal and the ligand in *trans*. Moreover, with the exception of **3IPF$_6$** showing a slightly longer Au-N^{pyrR} bond length (2.07 Å) compared to other $[(C^N^C)Au(pyrR)]^+$ complexes, no significant effect of the pyridine could be observed on the Au-N^{pyrR} bond length in any of the three complexes series we studied. Altogether, these data suggest that Au-N^{pyrR} bond length measurements are suitable to evaluate *trans* influence of the different scaffolds with the N-donor having a lower *trans* influence than the aryl ligand as reported in the literature[23] whereas it seems not suitable for discriminating *cis* influence and substituent effects.

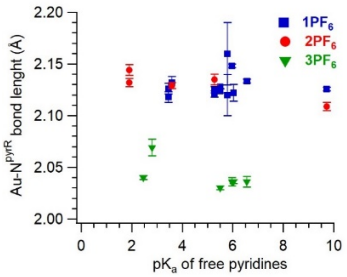

Figure 2. Relation between the Au-N^{pyrR} bond length measured by X-ray diffraction and the pK$_a$ of the corresponding free pyridines.

^{1}H NMR analysis. Another classical descriptor of the electronic influence of ligand is the ^{1}H NMR shift difference which can be observed upon coordination of the ligand and which can be linked to the ligand donation capability towards the metal. Previous works on Pt(II) and Pd(II) complexes bound to substituted pyridines have also reported on the linear correlation observed between the pK$_a$ values of the free pyridines and the shift of the ^{1}H NMR chemical shift ($\Delta\delta$) of the pyridinic protons upon coordination with the metals.[31, 32] This comparison between the chosen descriptor (^{1}H $\Delta\delta$) and the pK$_a$ appeared very interesting to us as pK$_a$s are directly reflecting the donating capability of the pyridine and are easily manipulated by chemists. A similar analysis was accordingly undertaken on our Au(III) complexes. First, as seen in Fig. 3A, the ^{1}H shifts measured for pyridinic H2/H6 and H3/H5 protons show a nearly linear dependence with ^{1}H shifts of free pyridines. This indicates that the decrease in the electron density of the pyridinic protons is following the same trend upon coordination. Furthermore, the change in chemical shifts upon coordination was calculated and it appeared more pronounced on the *meta* protons (H3/H5) than on the *ortho* (H2/H6) ones, as already observed in the literature for Au(III) complexes (Fig. 3B and C).[33] This behavior is specific to Au(III), as Pt(II) and Pd(II) complexes exhibit, on the contrary, the highest deshielding on the H2/H6 pyridinic protons upon coordination.

Complexes **1PF$_6$** and **3PF$_6$** show the largest shifts on the H3/H5 protons, between 0.35 and 0.80 ppm for the *meta* ^{1}H position *vs.* 0.1-0.5 ppm for the *ortho* one. On the other hand, complexes **2PF$_6$** lead to a relatively small deshielding of the pyridines protons (below 0.3 ppm). This feature is attributed to the interaction taking place between the pyridine and the aromatic ring of the PPh$_3$ ligand as observed on the X-ray structures. Confronting these $\Delta(\delta)$ values with the pK$_a$ of the free pyridines indicates that only the **2PF$_6$** H2/H6 ^{1}H $\Delta(\delta)$ exhibit an almost linear dependence to the pK$_a$s (R^2 = 0.991, Fig. 3B)). In this series, on the contrary to the others, only *para* substituted pyridines have been considered, as for the work of Kurpik *et al.*[31] and Lewis *et al.*,[32] which may explain this result. Changing the substituent from the *para* to the *meta* or *ortho* position on the pyridine possibly increases the steric interaction between the pyridine and the scaffold and thus affects the chemical shift of the pyridine protons. Accordingly, as pyridines **j**-**n** with substituents in position 2 and 3 have been considered for the scaffolds **1** and **3**, the correlation between ^{1}H NMR $\Delta(\delta)$ and pK$_a$s appears to be very poor (R^2 < 0.6). Note however that the H2/H6 and H3/H5 ^{1}H $\Delta(\delta)$ of complexes **1** and **3** with only *para* substituted pyridines still do not relate well to the pK$_a$s (R^2 < 0.8, not shown), indicating that besides the position of the pyridine substituent, other factors influence the chemical shift of the protons of the pyridine ring and thus hinder the direct measurement of the electronic effect induced by the pyridine on Au(III) complexes. Thus, on the contrary on Pt(II) and Pd(II) complexes, ^{1}H NMR shifts may not serve as a reliable descriptor to evaluate the ligand donating effect on Au(III) complexes.

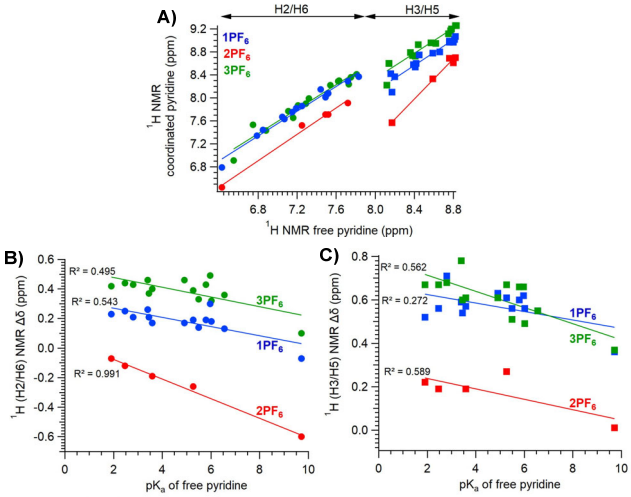

Figure 3. A) Relation between the ^{1}H NMR shifts of the H2/H6, H3/H5 protons of coordinated and free pyridines (almost-linear dependence (R^2> 0.90)). Shift of the ^{1}H NMR shift between the pyridinic proton in position **B)** 2/6 or **C)** 3/5 of the coordinated pyridines *vs.* the pk$_a$ of the free pyridines. For R substituents in *ortho* or *meta* position (pyridines **k**-**n**), the most deshielded proton was considered.

Bond dissociation energy measurements. Besides bond lengths or ^{1}H NMR shifts, other experimental descriptors may serve to evaluate the donating capability of a ligand. This can for instance be the case of the bond strength value between the metal and the ligand. Previous works in our group have already shown the capability of bond dissociation energies (BDEs) to efficiently evaluate *trans* ligand effect on Au(I) complexes.[13, 14] Following these results, it appeared interesting to probe BDE as a descriptor of the Au(III)-pyridine interaction. To this end, the Au-pyridine bond strength of the 3 series of complexes were experimentally determined using a mass spectrometry (MS) - based approach. MS is a very valuable tool for the determination of thermochemical quantities. As the complexes under study already bear a positive charge, the experimental method to determine the Au(III) - pyridines critical energies were

relatively easy to setup. By using collisional activation, performed in the HCD cell of an Orbitrap and under the multi-collisional regime in our case, it is thus possible to obtain survival yields over a large collision energy range. This yield represents the ratio of the intensity of the precursor ion over the sum the intensity of the precursor and the fragments. As simple way to compare bond strengths within the series of complexes would first consist in determining the energy required to fragment 50% of the precursor signal or to determine the extrapolation of the fragmentation onset from the fragment ion curve (see for instance ref. [34]). These procedures are often used for qualitative studies and have the advantage to be obtained directly from the energy-resolved mass spectra. The derived energies are however only relative and to obtain critical energies in an absolute scale, a thorough kinetic modeling of the process is required. Note that the thermochemical quantity obtained is a critical energy E_0 which refers to the energy difference between the transition state of dissociation and the precursor ion at 0 K. Electronic structure calculations usually provide bond dissociation energies (BDEs) which correspond to the enthalpy change of the dissociation reaction at 0 K. For processes occurring without reverse activation energy, E_0 and BDE are very close and can be directly compared. This will be the case in the present study for a direct cleavage mechanism.

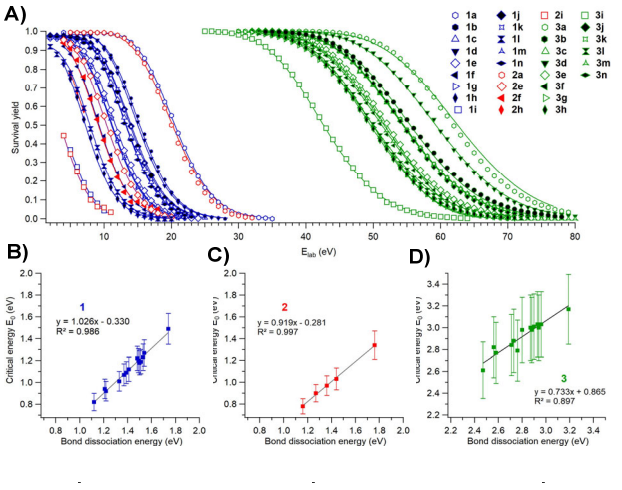

Figure 4. A) Experimental (markers) and modeled (lines) survival yield curves (SY) obtained for the set of 33 complexes. The relation between measured critical energies (± 1σ) and calculated bond-dissociation energies (with the ***M06*** method, see SI) is displayed for each family of complexes in **B)**, **C)** and **D)**.

In a previous work, Bayat *et al.*[35] proposed a kinetic model, based on RRKM theory[24-27] and using *MassKinetics* software,[36] to extract critical energy (E_0) from HCD fragmentation curves. In this approach, a calibration of the internal energy distribution deposited during the HCD experiment is performed and a linear relationship between the average internal energy of the ions $\langle E_{int} \rangle$ and the collision energy in the laboratory frame (E_{lab}) is established for a model complex used as a reference (see SI for more details) and for which an initial guess of its critical energy has to be made. Following this approach, Bayat et al. were able to obtain a set of critical energies for ten hemicryptophane-guest complexes in excellent agreement with previously published data. In the present work, we first applied this approach but it was however not as satisfying because of the large differences in size or bond strength of our complexes which would have required an adjustment of the $\langle E_{int} \rangle = f(E_{lab})$ relationship for each complex. Starting from there, we developed a new kinetic model shortly described here (and in details in the SI). For each complex, the average internal energy $\langle E_{int} \rangle$ and its corresponding characteristic temperature T_{char} are obtained by assuming a collision process in which all of the kinetic energy of the precursor ion is converted into internal energy after a certain number of collisions. This number varies for each complex and depends on E_{lab}, on the effective collision cross section of each complex which are determined by ion mobility experiments and on the inelasticity coefficient (Eta) specific to each complex. This approach has the great advantage to be independent for any calculated BDEs values used as references on the contrary to the model developed by Bayat *et al.*[35] Therefore, it does not suffer from the lack of precision that may be encountered with the choice of the theoretical method to calculate thermochemistry data for the reference ion.

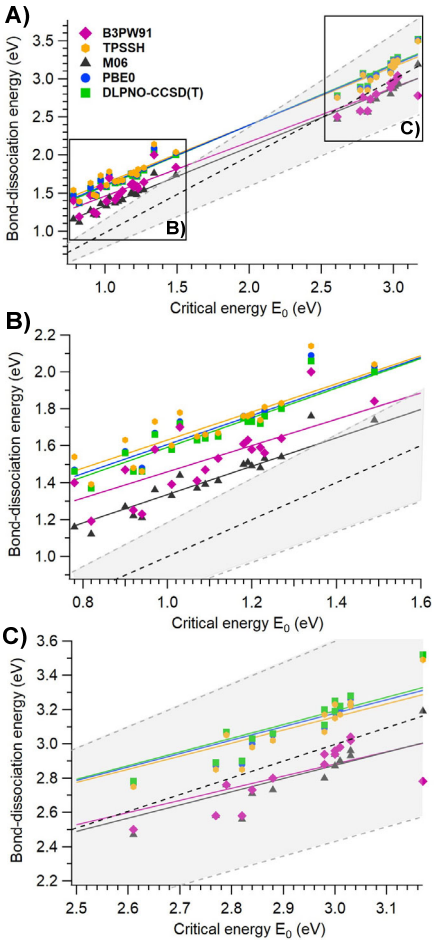

Figure 5. Calculated bond-dissociation energies determined with the 5 theoretical approaches (markers) and linear fit BDE = $f(E_0)$ obtained for each method (colored full lines). The black dotted line indicates the experimentally-determined critical energies and the grey area, the ± 2σ error estimated for this value. In **A)**, the whole set of values is displayed, in **B)** and **C)**, the BDEs range < 1.6 eV and > 2.5 eV are zoomed.

The survival yield curves obtained for the 33 complexes are displayed in Fig. 4A. Following the kinetic modeling, a set of 33 critical energies was obtained and is given in Table 1. Two distinct E_0 ranges appear depending on the complex scaffolds: below 1.5 eV for complexes **1** and **2** and above 2.5 eV for complexes **3**. These values agree well with the Au-N^{pyrR} bond lengths determined by X-ray diffraction and with the

observation that complexes **3** show a stronger Au-N^{pyrR} bonding than the two other series.

Table 1. pK_a values of the free pyridines, E_0 values (eV) measured by HCD-MS and calculated BDE (*M06)* (eV) for the 33 complexes.

Complex	R	pK_a[a]	E_0[b]	BDE
1a	4-NMe2	9.71	1.49 ± 0.14	1.74
1b	4-OMe	6.55	1.27 ± 0.12	1.54
1c	4-Me	6.02	1.18 ± 0.11	1.50
1d	4-Ph	5.49	1.23 ± 0.12	1.53
1e	H	5.27	1.12 ± 0.11	1.41
1f	4-Ac	3.59	1.01 ± 0.09	1.33
1g	4-CO2Et	3.45	1.07 ± 0.10	1.37
1h	4-CF3	2.46	0.92 ± 0.09	1.22
1i	4-CN	1.90	0.82 ± 0.08	1.12
1j	3-OMe	4.91	1.20 ± 0.11	1.49
1k	3-Me	5.79	1.22 ± 0.11	1.48
1l	3-CF3	2.80	0.94 ± 0.09	1.21
1m	2-OMe	3.40	1.09 ± 0.10	1.39
1n	2-Me	5.97	1.19 ± 0.11	1.51
2a	4-NMe2	9.61	1.34 ± 0.13	1.76
2e	H	5.23	1.03 ± 0.10	1.44
2f	4-Ac	3.57	0.97 ± 0.09	1.36
2h	4-CF3	2.46	0.90 ± 0.08	1.27
2i	4-CN	2.46	0.78 ± 0.07	1.16
3a	4-NMe2	9.61	3.17 ± 0.32	3.19
3b	4-OMe	6.47	3.03 ± 0.30	2.96
3c	4-Me	5.98	3.01 ± 0.30	2.90
3d	4-Ph	5.55	3.00 ± 0.30	2.94
3e	H	5.23	2.98 ± 0.30	2.80
3f	4-Ac	3.57	2.84 ± 0.28	2.71
3g	4-CO_2Et	3.45	2.79 ± 0.28	2.76
3h	4-CF_3	2.46	2.77 ± 0.28	2.58
3i	4-CN	2.10	2.61 ± 0.26	2.47
3j	3-OMe	4.91	2.98 ± 0.30	2.88
3k	3-Me	5.63	3.00 ± 0.30	2.87
3l	3-CF_3	2.80	2.82 ± 0.28	2.56
3m	2-OMe	3.06	2.88 ± 0.29	2.73
3n	2-Me	6.00	3.03 ± 0.30	2.93

[a] Experimental or calculated pKa were obtained from ref. [37] (pyridines a, e, k), ref. [38] (pyridines b, c, g, j, m, n), ref. [39] (pyridine d), ref. [40] (pyridines f, i), ref. [32] (pyridine h) and ref. [41] (pyridine l). [b] The uncertainties given here correspond to 1 σ and were estimated by varying the different parameters used in the kinetic model (see SI for details).

To support and validate our experimental approach, an extensive theoretical work was undertaken. Several DFT approaches were chosen according to literature studies found on similar systems or describing their performance to access BDEs (see SI and ref. [42] for details of the calculations): B3PW91-D3(BJ)/SDD(+f) (Au), 6-31G** (other atoms), TPSSH-D3(BJ)/cc-pVTZ, M06/def2-TZVP and PBE0-D3(BJ)/def2-TZVP. They will be further termed according to the name of the functional used: B3PW91, TPSSH, M06 and PBE0. Domain-based local pair natural orbital coupled-cluster theory (DLPNO-CCSD(T)/cc-pVTZ termed further ***DLPNO-CCSD(T)***) was also used. BDEs were determined as the 0 K enthalpy change between the fragments and the precursor (including zero-point energy correction).

Comparison of the calculated BDEs with experimental E_0 is provided in Figure 5 and the mean and largest absolute deviations (resp. MAD and LAD), in Table 2 (all calculated values are given in Table S4). Globally, the fits between experiment and theory are quite good ($R^2 > 0.97$) with a slope of ca. 0.8 for all methods except for ***B3PW91***. Some discrepancies however appear depending on the family of complexes considered. Thus, families **1** and **2** present BDEs with the largest deviation to the E_0 values, with a LAD belonging to the complexes **2** for all theoretical approaches. On the other hand, BDEs of series **3** all fall within the error bar defined for the E_0. Among all DFT methods, the ***M06*** functional appears to provide the closest BDEs values to experiment with a MAD of 5.2 kcal/mol. Conversely, the ***DLPNO-CCSD(T)*** method exhibit results with a larger deviation (MAD of 9.6 kcal/mol). The non-negligible deviation of this approach for the determination of BDEs in transition-metal complexes has already been several times reported. In particular, Husch *et al.* also related similar divergence to experiment with ***DLPNO-CCSD(T)***.[43] By comparing the performance of various theoretical approaches for a various set of organometallics reactions, they for instance found a MAD larger than 18 kcal/mol for an Au(I) system. Validity of the theoretical approaches is difficult to assess because of the very large difference and performance reported in the literature. Altogether, the calculated BDEs however predict the same trend as experiment and are consistent together. In particular, the ***PBE0***, ***TPSSH*** and ***DLPNO-CCSD(T)*** methods present very close agreement.

To summarize, a global shift of about 0.3 eV (7 kcal/mol) is obtained between theory and experiment. The largest deviation to theory is obtained for complexes **1** and **2**, although they are the experimental data obtained with the highest precision (see Fig. 4B), C) and D)). A possible explanation for this shift is related to the choice of the transition states (TS). A TS treated at the phase space limit (PSL) may have been relevant and would have probably produce higher values of E_0, this TS being product-like.[44] However this approach is not available in *MassKinetics* software. On the other hand, the calculated BDEs also appear to be overestimated. For instance, the calculated BDEs for **1i** vary between 1.12 eV and 1.53 eV depending on the methods used which seems high considering that this compound is decomposed at 63% for a collision voltage of 5 V. In the case of family **3**, the modeling of the curves was more complex due to consecutive and competitive fragmentations with the most abundant fragment being not always the pyridine loss. Despite this shift, the correlation experiment/theory remains very satisfying and help comforting the validity of our kinetic model.

To follow up on the evaluation of the ligand influence on the Au-N^{pyrR} bond strength, we compared the determined critical energies with the pK_a of the corresponding free pyridines (Figure 6). Very interestingly, an almost-linear dependence with the pK_as appeared for the three scaffolds together ($R^2 > 0.88$). This indicates that the critical energies can be directly related to the donating capability of the pyridine and do not depend on the substituent position on the pyridine. They can be applied over a large range of bonding strength, from the most fragile complexes **1** and **2** up to the strongest ones, complexes **3**. This

Table 2. Mean and largest absolute deviations (resp., MAD and LAD in kcal/mol) to E_0 obtained for the 5 theoretical methods used. The data are given for the whole set of complexes and for each series. The equation of the linear fit BDE = f(E_0) (in eV) displayed in Fig. 5 and the determination coefficient are also given.

	MAD (LAD)				Equation of the fit
	1	2	3	All	y = ax + b (R^2)
B3PW91	8.5 (10.1)	14.4 (15.4)	2.4 (9.1)	6.8	y = 0.712x + 0.74705 (R^2 = 0.9693)
TPSSH	12.9 (13.5)	17.5 (18.5)	3.8 (7.3)	19.8	y = 0.763x + 0.8678 (R^2 = 0.9833)
M06	6.2 (7.3)	9.1 (9.6)	2.8 (6.0)	5.2	y = 0.770x + 0.5643 (R^2 = 0.9901)
PBE0	12.7 (13.3)	16.2 (17.2)	4.3 (7.9)	9.7	y = 0.786x + 0.82068 (R^2 = 0.9879)
DLPNO-CCSD(T)	12.4 (13.2)	15.8 (16.5)	4.6 (8.1)	9.6	y = 0.801x + 0.79026 (R^2 = 0.9897)

underline the more global character of this descriptor in contrast with the ^{1}H NMR chemical shift analysis which could only provide reliable results for a restrained range of Au-pyrR interaction (same scaffold). Moreover, for the three families of complexes, the differences between the most stable and the most fragile complexes are rather equivalent: ca 0.6 eV for the three series. This suggest that the substituents on the pyridine have similar impact of the Au-pyrR bond whatever the considered Au(III) scaffold. Furthermore, the difference observed between the $[(C\hat{}C)Au(NHC)(pyrR)]^+$ and $[(C\hat{}N\hat{}C)Au(pyrR)]^+$ complexes remains constant for each pyridine with an average value of 1.80 eV. This value can be seen as a quantification by means of bond strength of the difference in the *trans* influence of an aryl group and a N-donor group. One can also further notice that the replacement of the NHC ligand by a PPh_3 is leading to slightly lower E_0 values which can be attributed to a greater sterical hindrance of the PPh_3 ligand when compared to the NHC, thus weakening the bonding between the pyridine and the metal (families **1** and **2**, Fig. 6). The magnitude of this decrease appeared very dependent of the pyridine ligand with the most electron-rich pyridine being the most impacted by this effect (ΔE_0 = -0.15, -0.09 and -0.04 eV between **1a** and **2a**, **1e** and **2e** and **1i** and **2i**, respectively). One can tentatively rationalize these results considering the π-stacking observed in the crystal structures of $[(C\hat{}C)Au(PPh_3)(pyrR)]^+$ complexes between the pyridines and a phenyl ring of the PPh_3 ligand. This interaction is stronger with electron-poor pyridine ligands and partially compensates the sterical hindrance of the PPh_3 in good agreement with the greater downfield shift of the ^{1}H NMR signals observed for complexes **2fPF$_6$**, **2hPF$_6$** and **2iPF$_6$** (figure 4B,C).

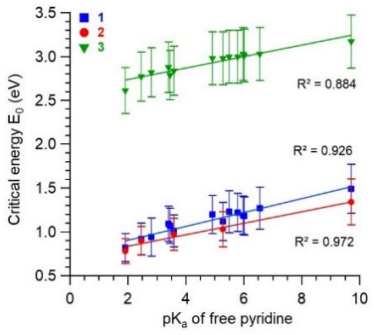

Figure 6. Relation between the critical energies determined for the 33 Au(III) complexes (± 1σ) and the pK_a of the corresponding free pyridines.

These results are also in good agreement with the results obtained for Au-N^{pyrR} distances measured by X-ray diffraction analysis (Fig. 3, Table 1) for which we observed a clear discrimination due to the *trans* influence of the scaffold but not between the $[(C\hat{}C)Au(NHC)(pyrR)]^+$ and $[(C\hat{}C)Au(PPh_3)(pyrR)]^+$ complexes or between the members of a given family. Combined together, these results enable us to decompose the various contributions of the different part of the complexes into the Au-pyridine dissociation energy: the main contribution comes from *trans* influence of the chelating ligand as was observed for Au(III)-H complexes,[7] then comes the substituent effect on the pyridine ligands and finally comes the impact of the *cis* ligand.

π-backdonation investigation. In the literature, the π-backdonation contribution in gold (I/III) complexes remains a debated topic.[45, 46] In Au(I) complexes, theoretical studies have suggested important contribution of π-backdonation in the Au-C bond strength in acetylene,[47] CO[48] and NHC[49] complexes. However, most of the time, no experimental observation of this π-backdonation could be made.[48, 50] Bourissou reported one of the sole experimental example of an Au(I) complex exerting π-backdonation by using a trigonal Au(I) scaffold with a chelating diphosphine ligand.[51] Furthermore, isolobality between cationic Au(I) and proton has already been stated[52] and points thus toward the poor contribution of π-backdonation in gold(I) complexes. A similar analogy is missing for Au(III) complexes although it could bring valuable information on the involvement of π-backdonation in Au(III) chemistry. Theoretical studies pointed to the involvement of π-backdonation in Au(III)-CO and alkyne bonds,[53-55] however, due the low stability of Au(III)-CO and alkyne complexes, very few Au(III) carbonyl or alkyne complexes are reported so far,[7, 56, 57] and thus investigation of π-backdonation in Au(III) complexes are scarce. Whereas variably reliable or no correlation could be observed between pK_a and ^{1}H NMR data and the Au-N^{pyrR} bond length, a reliable linear correlation was evidenced for the three scaffolds by considering the Au-N^{pyrR} E_0 with very similar slopes observed for the corresponding linear regression curves. These results indicate an analogous behavior of the cationic Au(III) scaffolds towards coordination with pyridines and this may suggest the isolobality of these three cationic organogold(III) scaffolds with protons. To investigate in more detail this feature, a closer look was taken on the Au-N^{pyrR} interaction by using an energy decomposition analysis (EDA). This theoretical approach enables a quantitative description and decomposition of the various energetics terms involved in the bonding between two fragments, the Au(III) scaffold and the pyridine here. These terms are the global interaction energy ΔE_{int} which is decomposed into a repulsive (Pauli repulsion, ΔE_{Pauli}) and two attractive terms responsible for the electrostatic (ΔE_{elect}) and the orbital (ΔE_{orb}) interaction. They are displayed in Fig. S25 vs. the critical energy E_0 of the complexes and the values are given in the SI (Table

S8). All four terms have an almost linear dependence towards the BDEs. The interaction energy is predicted larger for the complexes 3 in agreement with the measured E_0s and BDEs. For the three series, the contribution of the electrostatic attraction in the total attractive interactions for the Au(III) complexes is larger (ca 65%) than the covalent (orbital) ΔE_{orb} binding (ca 35%). This results agrees well with previous theoretical work of Radenković et al. on Au–N bonding in Au(III) complexes.[58]64 Using various theoretical approaches, they indeed determined that the bonding between Au(III) and N-containing heterocycles has a higher electrostatic than covalent character.

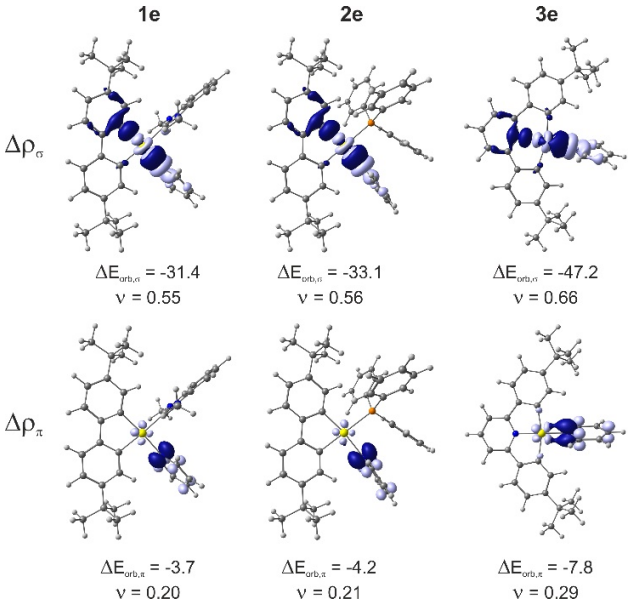

Figure 7. Contours of deformation density $\Delta\rho_\sigma$ and $\Delta\rho_\pi$ connected with the pairs of interacting orbitals in the **1e**, **2e** and **3e** complexes. The surfaces in light purple represent an electron density loss and in dark blue, an electron density gain. The associated orbital interaction energies ΔE_{orb} are given in kcal/mol, ν is the eigenvalue indicating the size of the charge flow. Isosurface value: 0.0025 a.u.

The ΔE_{orb} contribution can be further decomposed using the NOCV approach (natural orbitals for chemical valence). This enables to obtain the main deformation densities contributing to the orbital interaction on the Au-N^{pyrR} bond. For each family of complexes, an example of the NOCV results is displayed in Fig. 7 and the results for all complexes in Table S9. Two main contributions accounting for more than 80% are observed, showing that the Au-N^{pyrR} bonding exhibits mostly a σ-donor and a π-acceptor character ($\Delta\rho_\sigma$ and $\Delta\rho_\pi$, ca 70% and 10 % of the contribution, respectively). Altogether, these results point toward a limited involvement of the π-backdonation in good agreement with the similar linear correlation between the E_0s of the complexes for the three families and the pK_as of the pyridines.

Application to catalysis. As seen, the donating capability of the pyridines described by their pK_as exhibits a close dependence to the Au-N^{pyrR} bond dissociation energies. In a further step, we wished to confront these results with a catalytic application to determine in which extent the ligand donor effect may be related to catalytic efficiency of the corresponding complexes. We focused on the well-known Lewis acid properties of gold complexes which can thus act as catalysts to activate C-C multiple bonds toward nucleophilic attacks.[59, 60] In particular, Toste has reported the use of a $[(C\hat{}C)Au(NHC)]^+$ cation (generated by chloride abstraction from the corresponding [(C^C)Au(NHC)Cl] complex) for an enantioconvergente cycloisomerization reaction of enynes.[61] Moreover, 8-hydroxyjuloludinyl phenylpropiolate has been reported to be efficiently converted to the corresponding coumarin *via* a gold-catalyzed intramolecular hydroarylation reaction.[62, 63] Within this context, we decided to apply our Au(III)-pyridine complexes in the intramolecular hydroarylation reaction of 8-hydroxyjuloludinyl phenylpropiolate (Fig. 8A)). We reacted the substrate with 2.5 mol% of Au(III) complexes in $CDCl_3$ at room temperature for 6 h and calculated the conversion rate using ^{1}H NMR spectroscopy. Considering that the decoordination of the pyridine ligands would generate the catalytically active species similar to Toste's systems, we correlated the conversion rate of the reaction with the dissociation energies we measured for the complexes (Fig. 8 and table S10).

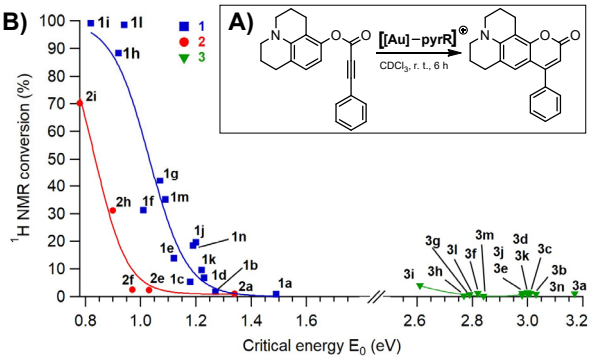

Figure 8. **A)** Conversion reaction scheme of 8-hydroxyjuloludinyl phenylpropiolate catalyzed by the studied Au(III) complexes and **B)** relation between the determined ^{1}H NMR conversion of the reaction (%) and the critical energies of the Au(III) complexes.

For the (C^C)-based complexes **1a-n** and **2a, e, f, h, i**, a correlation between the dissociation energy of the pyridine ligand and the conversion rate is observed. In both cases, the conversion rate is indeed increasing when the dissociation energy decreases. In the series of complexes **1a-n**, the conversion rate evolves from almost no conversion for the most stable complex (0.8 % conversion for complex **1a**) to almost complete conversion for the complex with the most labile pyridine ligand (99 % conversion for complex **1i**). The same trend is observed in the complexes **2** series with the most stable complex **2a** giving only 1.1 % conversion and complex **2i**, with the most labile pyridine ligand, leading to 70 % conversion. Within each family of complexes, the same catalytically active species is formed upon decoordination of the pyridine ligands, ie. $[(C\hat{}C)Au(NHC)]^+$ and $[(C\hat{}C)Au(PPh_3)]^+$ for complexes **1a-n** and **2a, e, f, h, i**, respectively. As such, the more labile the pyridine is, the more the catalytically active species is generated leading to a higher conversion rate. For the (C^N^C)-based complexes, none of them showed any catalytic activity independently to the nature of the pyridine ligand suggesting that all are too stable to generate the catalytically active species. This is consistent with the determined E_0s showing that all (C^N^C)-based complexes are much more stable than all (C^C)-based ones. The dissociation energy between the pyridine ligand and Au(III) appears thus to be a key parameter for the conversion of the substrate as it enables the generation of the catalytically active species. Furthermore, it is worth noting that despite slightly lower dissociation energies of the pyridine ligands in the $[(C\hat{}C)Au(PPh_3)(pyrR)]^+$ series compared to the $[(C\hat{}C)Au(NHC)(pyrR)]^+$ analogues, complexes $[(C\hat{}C)Au(PPh_3)(pyrR)]^+$ lead to lower conversion rates (conversion rates of 70, 31 and 2.5 % for **2i**, **2h** and **2f**, respectively

compared to 99, 88 and 31 % for **1i**, **1h** and **1f**, respectively). This shows that the conversion rate is influenced by other parameters than the dissociation energies. After decoordination of the pyridines, the formed catalytically active species may exhibit different efficiencies leading thus to different reaction yields. In this particular case, the $[(C\hat{}C)Au(NHC)]^+$ species appears more efficient than the $[(C\hat{}C)Au(PPh_3)]^+$ analog. We compared the geometry optimized structures of the $[(C\hat{}C)Au(NHC)]^+$ and $[(C\hat{}C)Au(PPh_3)]^+$ scaffolds. Interestingly, a large difference is observed in the access angle of the substrate to the Au(III) center due to the larger steric influence of PPh_3 compared to the planar NHC (resp. 10° *vs*. 113°, Fig. S27). As such, although electronic differences between the two active species should not be ruled out, sterical hindrance around the gold center in the active species seems to be the discriminating parameter. Indeed, the coordination of the C-C triple bond to the Au(III) center which is the first step of the catalytic cycle (Fig. S27C)), might be disfavored in the case of the $[(C\hat{}C)Au(PPh_3)]^+$ species leading to a reduced conversion of the substrate. This feature illustrates the role that steric effect may play in complement to pure electronic influence of the ligand.

CONCLUSIONS

We report in this work the synthesis of 33 new organogold complexes based on three different scaffolds $[(C\hat{}C)Au(NHC)(pyrR)]^+$, $[(C\hat{}C)Au(PPh_3)(pyrR)]^+$ and $[(C\hat{}N\hat{}C)Au(pyrR)]^+$. These complexes have been used for the development of a first direct and absolute experimental methodology for the determination of metal-ligand dissociation energies using an HCD-based mass spectrometry approach over a large dissociation energy range. Confrontation of the results with several theoretical methods demonstrate the high reliability of the results obtained and the ability of this approach to describe simultaneously very different systems by means of sizes and strengths, on the contrary to classical methodologies based on NMR spectroscopy and crystal structure analysis. Further analysis on the Au-pyrR interaction using the EDA scheme could demonstrate a low contribution of the π-backdonation for all systems and thus the isolobality of the different Au(III) scaffolds with proton. Additionally, the catalytic activity of the complexes was determined in an alkyne intramolecular hydroarylation reaction. Rationalizing the results in light of the complexes critical energies could help to discriminate the systems limited by the activation of the pre-catalyst from the systems limited by the reactivity of the catalytic species. Altogether, these data highlight the great potential of this gas-phase methodology and of the metal-ligand dissociation energy as a reliable ligand effect descriptor. It could help to access a better comprehension of the intramolecular interactions and of the condensed-phase activity of organometallics. Furthermore, if the proposed methodology requires specific instruments and kinetic modelization tools, relative M-L bond strengths can be easily accessed with a good precision from simplified MS analysis ($E_{1/2}$) or by theory, enabling thus an universal access to the methodology.

ASSOCIATED CONTENT

Supporting Information

The Supporting Information is available free of charge on the ACS Publications website.
Supplementary Informations_final.pdf

AUTHOR INFORMATION

Corresponding Authors

* Denis Lesage: Sorbonne Université, CNRS, Institut Parisien de Chimie Moléculaire (IPCM UMR 8232), F-75005 Paris, France
Email: denis.lesage@sorbonne-universite.fr
* Benoît Bertrand: Sorbonne Université, CNRS, Institut Parisien de Chimie Moléculaire (IPCM UMR 8232), F-75005 Paris, France
Email: benoit.bertrand@sorbonne-universite.fr
* Héloïse Dossmann: Sorbonne Université, CNRS, Institut Parisien de Chimie Moléculaire (IPCM UMR 8232), F-75005 Paris, France
Email: heloise.dossmann@sorbonne-universite.fr

Author Contributions

The manuscript was written through contributions of all authors. All authors have given approval to the final version of the manuscript.

ACKNOWLEDGMENT

This work was granted access to the HPC resources of the SACADO MeSU platform at Sorbonne Université. HD, BB and DL thanks CNRS and Sorbonne Université for financial support, LB thanks the Labex MiChem and the SOLEIL synchrotron facility for PhD funding. SS grateful acknowledged Erasmus+ for a traineeship funding.

REFERENCES

(1) Alvarez, S.; Palacios, A. A.; Aullón, G. Ligand orientation effects on metal–metal, ligand–ligand and metal–ligand interactions. *Coord. Chem. Rev.* **1999**, *185-186*, 431-450. DOI:10.1016/S0010-8545(99)00027-2.

(2) Marks, T. J.; Gagne, M. R.; Nolan, S. P.; Schock, L. E.; Seyam, A. M.; Stern, D. What can metal-ligand bonding energetics teach us about stoichiometric and catalytic organometallic chemistry? *Pure Appl. Chem.* **1989**, *61* (10), 1665-1672. DOI:10.1351/pac198961101665.

(3) Constable, E. C. *Metals and Ligand Reactivity: An Introduction to the Organic Chemistry of Metal Complexes*; Wiley, 1995.

(4) Tolman, C. A. Electron donor-acceptor properties of phosphorus ligands. Substituent additivity. *J. Am. Chem. Soc.* **1970**, *92* (10), 2953-2956. DOI:10.1021/ja00713a006.

(5) Dröge, T.; Glorius, F. The Measure of All Rings-N-Heterocyclic Carbenes. *Angew. Chem. Int. Ed.* **2010**, *49* (39), 6940-6952. DOI:10.1002/anie.201001865.

(6) Teng, Q.; Huynh, H. V. A unified ligand electronic parameter based on 13C NMR spectroscopy of N-heterocyclic carbene complexes. *Dalton Trans.* **2017**, *46* (3), 614-627, 10.1039/C6DT04222H. DOI:10.1039/C6DT04222H.

(7) Rocchigiani, L.; Bochmann, M. Recent Advances in Gold(III) Chemistry: Structure, Bonding, Reactivity, and Role in Homogeneous Catalysis. *Chem. Rev.* **2021**, *121* (14), 8364-8451. DOI:10.1021/acs.chemrev.0c00552.

(8) Dossmann, H.; Gatineau, D.; Clavier, H.; Memboeuf, A.; Lesage, D.; Gimbert, Y. Exploring Phosphine Electronic Effects on Molybdenum Complexes: A Combined Photoelectron Spectroscopy and Energy Decomposition Analysis Study. *J. Phys. Chem. A* **2020**, *124* (42), 8753-8765. DOI:10.1021/acs.jpca.0c06746.

(9) Green, J. C. Photoelectron Spectroscopy. In *Comprehensive Organometallic Chemistry III*, Elsevier, 2007; pp 381-406.

(10) Head, A. R.; Renshaw, S. K.; Uplinger, A. B.; Lomprey, J. R.; Selegue, J. P.; Lichtenberger, D. L. Experimental measure of metal–alkynyl electronic structure interactions by photoelectron spectroscopy: (η5-C5H5)Ru(CO)2C CMe and [(η5-C5H5)Ru(CO)2]2(μ-C C). *Polyhedron* **2015**, *86*, 141-150. DOI:10.1016/j.poly.2014.07.020.

(11) Armentrout, P. B. Gas-Phase Organometallic Chemistry. In *Organometallic Bonding and Reactivity*, Brown, J. M., Hofmann, P. Eds.; Vol. 4; Springer Berlin Heidelberg, 1999; pp 1-45.

(12) Pongor, C. I.; Szepes, L.; Basi, R.; Bodi, A.; Sztáray, B. Metal–Carbonyl Bond Energies in Phosphine Analogue Complexes of $Co(CO)_3NO$ by Photoelectron Photoion Coincidence Spectroscopy. *Organometallics* **2012**, *31* (9), 3620-3627. DOI:10.1021/om300132g.

(13) Gatineau, D.; Dossmann, H.; Clavier, H.; Memboeuf, A.; Drahos, L.; Gimbert, Y.; Lesage, D. Ligand effects in gold-carbonyl complexes: Evaluation of the bond dissociation energies using blackbody infrared radiative dissociation. *Int. J. Mass spectrom.* **2021**, *463*, 116545. DOI:10.1016/j.ijms.2021.116545.

(14) Gatineau, D.; Lesage, D.; Clavier, H.; Dossmann, H.; Chan, C. H.; Milet, A.; Memboeuf, A.; Cole, R. B.; Gimbert, Y. Bond dissociation energies of carbonyl gold complexes: a new descriptor of ligand effects in gold(i) complexes? *Dalton Trans.* **2018**, *47* (43), 15497-15505, 10.1039/C8DT03721C. DOI:10.1039/C8DT03721C.

(15) Bertrand, B.; O'Connell, M. A.; Waller, Z. A. E.; Bochmann, M. A Gold(III) Pincer Ligand Scaffold for the Synthesis of Binuclear and Bioconjugated Complexes: Synthesis and Anticancer Potential. *Chem. Eur. J.* **2018**, *24* (14), 3613-3622. DOI:10.1002/chem.201705902.

(16) Williams, M.; Green, A. I.; Fernandez-Cestau, J.; Hughes, D. L.; O'Connell, M. A.; Searcey, M.; Bertrand, B.; Bochmann, M. $(C^N^{pz}^C)Au^{III}$ complexes of acyclic carbene ligands: synthesis and anticancer properties. *Dalton Trans.* **2017**, *46* (39), 13397-13408. DOI:10.1039/C7DT02804K.

(17) Chambrier, I.; Hughes, D. L.; Jeans, R. J.; Welch, A. J.; Budzelaar, P. H. M.; Bochmann, M. Do Gold(III) Complexes Form Hydrogen Bonds? An Exploration of AuIII Dicarboranyl Chemistry. *Chem. Eur. J.* **2020**, *26* (4), 939-947. DOI:10.1002/chem.201904790.

(18) Joost, M.; Amgoune, A.; Bourissou, D. Reactivity of Gold Complexes towards Elementary Organometallic Reactions. *Angew. Chem. Int. Ed.* **2015**, *54* (50), 15022-15045. DOI:10.1002/anie.201506271.

(19) Chan, K. T.; Tong, G. S. M.; Wan, Q.; Cheng, G.; Yang, C.; Che, C.-M. Strongly Luminescent Cyclometalated Gold(III) Complexes Supported by Bidentate Ligands Displaying Intermolecular Interactions and Tunable Emission Energy. *Chem. Asian J.* **2017**, *12* (16), 2104-2120. DOI:10.1002/asia.201700686.

(20) Wong, K. M.-C.; Hung, L.-L.; Lam, W. H.; Zhu, N.; Yam, V. W.-W. A Class of Luminescent Cyclometalated Alkynylgold(III) Complexes: Synthesis, Characterization, and Electrochemical, Photophysical, and Computational Studies of [Au(CΛNΛC)(C⋮CR)] (CΛNΛC = κ3C,N,C Bis-cyclometalated 2,6-Diphenylpyridyl). *J. Am. Chem. Soc.* **2007**, *129* (14), 4350-4365. DOI:10.1021/ja068264u.

(21) Yang, J.; Giuso, V.; Hou, M.-C.; Remadna, E.; Forté, J.; Su, H.-C.; Gourlaouen, C.; Mauro, M.; Bertrand, B. Biphenyl Au(III) Complexes with Phosphine Ancillary Ligands: Synthesis, Optical Properties, and Electroluminescence in Light-Emitting Electrochemical Cells. *Inorg. Chem.* **2023**, *62* (12), 4903-4921. DOI:10.1021/acs.inorgchem.2c04293.

(22) Fung, S. K.; Zou, T.; Cao, B.; Lee, P.-Y.; Fung, Y. M. E.; Hu, D.; Lok, C.-N.; Che, C.-M. Cyclometalated Gold(III) Complexes Containing N-Heterocyclic Carbene Ligands Engage Multiple Anti-Cancer Molecular Targets. *Angew. Chem. Int. Ed.* **2017**, *56* (14), 3892-3896. DOI:10.1002/anie.201612583.

(23) See, R. F.; Kozina, D. Quantification of the trans influence in d^8 square planar and d^6 octahedral complexes: a database study. *J. Coord. Chem.* **2013**, *66* (3), 490-500. DOI:10.1080/00958972.2012.758842.

(24) Kassel, L. S. Studies in Homogeneous Gas Reactions. I. *J. Phys. Chem.* **1928**, *32* (2), 225-242. DOI:10.1021/j150284a007.

(25) Marcus, R. A. Unimolecular Dissociations and Free Radical Recombination Reactions. *J. Chem. Phys.* **1952**, *20* (3), 359-364. DOI:10.1063/1.1700424.

(26) Marcus, R. A.; Rice, O. K. The Kinetics of the Recombination of Methyl Radicals and Iodine Atoms. *J. Phys. Chem.* **1951**, *55* (6), 894-908. DOI:10.1021/j150489a013.

(27) Rice, O. K.; Ramsperger, H. C. Theories of unimolecular gas reactions at low pressures. *J. Am. Chem. Soc.* **1927**, *49* (7), 1617-1629. DOI:10.1021/ja01406a001.

(28) David, B.; Monkowius, U.; Rust, J.; Lehmann, C. W.; Hyzak, L.; Mohr, F. Gold(iii) compounds containing a chelating, dicarbanionic ligand derived from 4,4′-di-tert-butylbiphenyl. *Dalton Trans.* **2014**, *43* (28), 11059-11066. DOI:10.1039/C4DT00778F.

(29) Bertrand, B.; Fernandez-Cestau, J.; Angulo, J.; Cominetti, M. M. D.; Waller, Z. A. E.; Searcey, M.; O'Connell, M. A.; Bochmann, M. Cytotoxicity of Pyrazine-Based Cyclometalated $(C^N^{pz}^C)Au(III)$ Carbene Complexes: Impact of the Nature of the Ancillary Ligand on the Biological Properties. *Inorg. Chem.* **2017**, *56* (10), 5728-5740. DOI:10.1021/acs.inorgchem.7b00339.

(30) Chambrier, I.; Rocchigiani, L.; Hughes, D. L.; Budzelaar, P. M. H.; Bochmann, M. Thermally Stable Gold(III) Alkene and Alkyne Complexes: Synthesis, Structures, and Assessment of the trans -Influence on Gold-Ligand Bond Enthalpies. *Chem. Eur. J.* **2018**, *24* (44), 11467-11474. DOI:10.1002/chem.201802160.

(31) Kurpik, G.; Walczak, A.; Gołdyn, M.; Harrowfield, J.; Stefankiewicz, A. R. Pd(II) Complexes with Pyridine Ligands: Substituent Effects on the NMR Data, Crystal Structures, and Catalytic Activity. *Inorg. Chem.* **2022**, *61* (35), 14019-14029. DOI:10.1021/acs.inorgchem.2c01996.

(32) Lewis, N. A.; Pakhomova, S.; Marzilli, P. A.; Marzilli, L. G. Synthesis and Characterization of Pt(II) Complexes with Pyridyl Ligands: Elongated Octahedral Ion Pairs and Other Factors Influencing ^{1}H NMR Spectra. *Inorg. Chem.* **2017**, *56* (16), 9781-9793. DOI:10.1021/acs.inorgchem.7b01294.

(33) Pazderski, L.; Toušek, J.; Sitkowski, J.; Maliňáková, K.; Kozerski, L.; Szłyk, E. Experimental and quantum-chemical studies of ¹ H, ¹³ C and ¹⁵ N NMR coordination shifts in Au(III), Pd(II) and Pt(II) chloride complexes with picolines: NMR studies of Au(III), pd(II), Pt(II) picoline-chloride complexes. *Magn. Reson. Chem.* **2009**, *47* (3), 228-238. DOI:10.1002/mrc.2378.

(34) Mehara, J.; Koovakattil Surendran, A.; van Wieringen, T.; Setia, D.; Foroutan-Nejad, C.; Straka, M.; Rulíšek, L.; Roithová, J. Cationic Gold(II) Complexes: Experimental and Theoretical Study**. *Chem. Eur. J.* **2022**, *28* (60). DOI:10.1002/chem.202201794.

(35) Bayat, P.; Gatineau, D.; Lesage, D.; Martinez, A.; Cole, R. B. Benchmarking higher energy collision dissociation (HCD) by investigation of binding energies of gas-phase host–guest complexes of hemicryptophane cages. *J. Mass Spectrom.* **2022**, *57* (9), e4879. DOI:https://doi.org/10.1002/jms.4879.

(36) Drahos, L.; Vékey, K. MassKinetics: a theoretical model of mass spectra incorporating physical processes, reaction kinetics and mathematical descriptions: MassKinetics: a theoretical model of mass spectra. *J. Mass Spectrom.* **2001**, *36* (3), 237-263. DOI:10.1002/jms.142.

(37) Essery, J. M.; Schofield, K. 769. The influence of steric factors on the properties of 4-aminopyridine derivatives. *J. Chem. Soc.* **1961**, 3939. DOI:10.1039/jr9610003939.

(38) Clarke, K.; Rothwell, K. 377. A kinetic study of the effect of substituents on the rate of formation of alkylpyridinium halides in nitromethane solution. *J. Chem. Soc.* **1960**, 1885. DOI:10.1039/jr9600001885.

(39) Sigel, H.; Wynberg, H.; Van Bergen, T. J.; Kahmann, K. Acidity Constants of the Thienyl- and Phenyl-Pyridines and Stability Constants of the Corresponding Copper (II) 1:1 Complexes. *Helv. Chim. Acta* **1972**, *55* (2), 610-613. DOI:10.1002/hlca.19720550233.

(40) Tehan, B. G.; Lloyd, E. J.; Wong, M. G.; Pitt, W. R.; Gancia, E.; Manallack, D. T. Estimation of pKa Using Semiempirical Molecular Orbital Methods. Part 2: Application to Amines, Anilines and Various Nitrogen Containing Heterocyclic Compounds. *Quant. Struct.-Act.Relat.* **2002**, *21* (5), 473-485. DOI:10.1002/1521-3838(200211)21:5<473::AID-QSAR473>3.0.CO;2-D.

(41) Estimated from SciFinder (https://scifinder-n.cas.org/) from calculation using Advanced Chemistry Development (ACD/Labs) Software V11.02 (© 1994-2023 ACD/Labs). (accessed.

(42) Dossmann, H.; et al. Theoretical evaluation of the ligand-metal interaction in organogold(III)-pyridines complexes; Institut Parisien de Chimie Moléculaire, Sorbonne Université, Recherche Data Gouv: 2023. https://entrepot.recherche.data.gouv.fr/privateurl.xhtml?token=fb64d035-495f-49a4-bbcb-7f7815c624e0.

(43) Husch, T.; Freitag, L.; Reiher, M. Calculation of Ligand Dissociation Energies in Large Transition-Metal Complexes. *J. Chem.*

Theory Comput. **2018**, *14* (5), 2456-2468. DOI:10.1021/acs.jctc.8b00061.

(44) Carpenter, J. E.; McNary, C. P.; Furin, A.; Sweeney, A. F.; Armentrout, P. B. How Hot are Your Ions Really? A Threshold Collision-Induced Dissociation Study of Substituted Benzylpyridinium "Thermometer" Ions. *J. Am. Soc. Mass Spectrom.* **2017**, *28* (9), 1876-1888. DOI:10.1007/s13361-017-1693-0.

(45) Benitez, D.; Shapiro, N. D.; Tkatchouk, E.; Wang, Y.; Goddard, W. A.; Toste, F. D. A bonding model for gold(I) carbene complexes. *Nat. Chem.* **2009**, *1* (6), 482-486. DOI:10.1038/nchem.331.

(46) Echavarren, A. M. Carbene or cation? *Nat. Chem.* **2009**, *1* (6), 431-433. DOI:10.1038/nchem.344.

(47) Bistoni, G.; Belpassi, L.; Tarantelli, F. Disentanglement of Donation and Back-Donation Effects on Experimental Observables: A Case Study of Gold–Ethyne Complexes. *Angew. Chem. Int. Ed.* **2013**, *52* (44), 11599-11602. DOI:https://doi.org/10.1002/anie.201305505.

(48) Dash, C.; Kroll, P.; Yousufuddin, M.; Dias, H. V. R. Isolable, gold carbonyl complexes supported by N-heterocyclic carbenes. *Chem. Commun.* **2011**, *47* (15), 4478-4480, 10.1039/C1CC10622H. DOI:10.1039/C1CC10622H.

(49) Hu, X.; Castro-Rodriguez, I.; Olsen, K.; Meyer, K. Group 11 Metal Complexes of N-Heterocyclic Carbene Ligands: Nature of the MetalCarbene Bond. *Organometallics* **2004**, *23* (4), 755-764. DOI:10.1021/om0341855.

(50) Baker, M. V.; Barnard, P. J.; Berners-Price, S. J.; Brayshaw, S. K.; Hickey, J. L.; Skelton, B. W.; White, A. H. Cationic, linear Au(i) N-heterocyclic carbene complexes: synthesis, structure and anti-mitochondrial activity. *Dalton Trans.* **2006**, (30), 3708-3715, 10.1039/B602560A. DOI:10.1039/B602560A.

(51) Joost, M.; Estévez, L.; Mallet-Ladeira, S.; Miqueu, K.; Amgoune, A.; Bourissou, D. Enhanced π-Backdonation from Gold(I): Isolation of Original Carbonyl and Carbene Complexes. *Angew. Chem. Int. Ed.* **2014**, *53* (52), 14512-14516. DOI:https://doi.org/10.1002/anie.201407684.

(52) Raubenheimer, H. G.; Schmidbaur, H. Gold Chemistry Guided by the Isolobality Concept [†]. *Organometallics* **2012**, *31* (7), 2507-2522. DOI:10.1021/om2010113.

(53) Gaggioli, C. A.; Belpassi, L.; Tarantelli, F.; Belanzoni, P. The gold(iii)–CO bond: a missing piece in the gold carbonyl complex landscape. *Chem. Commun.* **2017**, *53* (10), 1603-1606, 10.1039/C6CC09879G. DOI:10.1039/C6CC09879G.

(54) Gregori, L.; Sorbelli, D.; Belpassi, L.; Tarantelli, F.; Belanzoni, P. Alkyne Activation with Gold(III) Complexes: A Quantitative Assessment of the Ligand Effect by Charge-Displacement Analysis. *Inorg. Chem.* **2019**, *58* (5), 3115-3129. DOI:10.1021/acs.inorgchem.8b03172.

(55) Sorbelli, D.; Belpassi, L.; Tarantelli, F.; Belanzoni, P. Ligand Effect on Bonding in Gold(III) Carbonyl Complexes. *Inorg. Chem.* **2018**, *57* (10), 6161-6175. DOI:10.1021/acs.inorgchem.8b00765.

(56) Ahrens, A.; Lustosa, D. M.; Karger, L. F. P.; Hoffmann, M.; Rudolph, M.; Dreuw, A.; Hashmi, A. S. K. Experimental and theoretical studies on gold(iii) carbonyl complexes: reductive C,H- and C,C bond formation. *Dalton Trans.* **2021**, *50* (25), 8752-8760. DOI:10.1039/D1DT01315G.

(57) Roşca, D.-A.; Fernandez-Cestau, J.; Morris, J.; Wright, J. A.; Bochmann, M. Gold(III)-CO and gold(III)-CO_2 complexes and their role in the water-gas shift reaction. *Sci. Adv.* **2015**, *1* (9), e1500761. DOI:10.1126/sciadv.1500761.

(58) Radenković, S.; Antić, M.; Savić, N. D.; Glišić, B. Đ. The nature of the Au–N bond in gold(iii) complexes with aromatic nitrogen-containing heterocycles: the influence of Au(iii) ions on the ligand aromaticity. *New J. Chem.* **2017**, *41* (21), 12407-12415, 10.1039/C7NJ02634J. DOI:10.1039/C7NJ02634J.

(59) Fürstner, A. Gold and platinum catalysis—a convenient tool for generating molecular complexity. *Chem. Soc. Rev.* **2009**, *38* (11), 3208-3221, 10.1039/B816696J. DOI:10.1039/B816696J.

(60) Zi, W.; Dean Toste, F. Recent advances in enantioselective gold catalysis. *Chem. Soc. Rev.* **2016**, *45* (16), 4567-4589, 10.1039/C5CS00929D. DOI:10.1039/C5CS00929D.

(61) Bohan, P. T.; Toste, F. D. Well-Defined Chiral Gold(III) Complex Catalyzed Direct Enantioconvergent Kinetic Resolution of 1,5-Enynes. *J. Am. Chem. Soc.* **2017**, *139* (32), 11016-11019. DOI:10.1021/jacs.7b06025.

(62) Vidal, C.; Tomás-Gamasa, M.; Destito, P.; López, F.; Mascareñas, J. L. Concurrent and orthogonal gold(I) and ruthenium(II) catalysis inside living cells. *Nat. Commun.* **2018**, *9* (1), 1913. DOI:10.1038/s41467-018-04314-5.

(63) Yang, Y.; Bai, B.; Jin, M.; Xu, Z.; Zhang, J.; Li, W.; Xu, W.; Wang, X.; Yin, C. Fluorescent imaging of Au^{3+} in living cells with two new high selective Au^{3+} probes. *Biosens. Bioelectron.* **2016**, *86*, 939-943. DOI:10.1016/j.bios.2016.07.112.